

Canonical Tail Dependence for Soft Extremal Clustering of Multichannel Brain Signals ¹

Mara Sherlin D.P. Talento^{a*}, Jordan Richards^{b**},

Raphaël Huser^{c*}, Hernando Ombao^{d*}

^a*marasherlin.talento@kaust.edu.sa*, ^b*jordan.richards@ed.ac.uk*,

^c*raphael.huser@kaust.edu.sa*, ^d*hernando.ombao@kaust.edu.sa*

*Statistics Program, Computer Electrical and Mathematical Science & Engineering,
King Abdullah University of Science and Technology

** School of Mathematics and Maxwell Institute for Mathematical Sciences,
University of Edinburgh, Edinburgh, UK, EH9 3FD

Abstract

We develop a novel characterization of extremal dependence between two cortical regions of the brain when its signals display extremely large amplitudes. We show that connectivity in the tails of the distribution reveals unique features of extreme events (e.g., seizures) that can help to identify their occurrence. Numerous studies have established that connectivity-based features are effective for discriminating brain states. Here, we demonstrate the advantage of the proposed approach: that tail connectivity provides additional discriminatory power, enabling more accurate identification of extreme-related events and improved seizure risk management. Common approaches in tail dependence modeling use pairwise summary measures or parametric models. However, these approaches do not identify channels that drive the maximal tail dependence between two groups of signals—an information that is useful when analyzing electroencephalography of epileptic patients where specific channels are responsible for seizure occurrences. A familiar approach in traditional signal processing is canonical correlation, which we extend to the tails to develop a visualization of extremal channel-contributions. Through the tail pairwise dependence matrix (TPDM), we develop a computationally-efficient estimator for our canonical tail dependence measure. Our method is then used for accurate frequency-based soft clustering of neonates, distinguishing those with seizures from those without.

Keywords: feature extraction; multivariate analysis; multivariate regular variation; representation learning; spectral analysis.

¹Preprint

1 Introduction

Early detection of seizures is crucial, especially at early ages where seizures pose a high risk of disrupting brain development. When unprovoked seizures occur in neonates, they often lead to epileptic encephalopathy (Mizrahi and Clancy, 2000), hence explaining why close monitoring in neonatal intensive care units (NICUs) is necessary. The primary modality for seizure management in an NICU is the electroencephalogram (EEG) (Sandoval Karamian and Wusthoff, 2021). However, even with medical-grade EEG technology, distinguishing neonates with seizures from those without (i.e., with normal ultrasound recordings) remains challenging, as the patterns and symptoms of seizures can appear deceptively similar (Stevenson et al., 2019). While our study is not directly aimed at detecting seizures, we develop a data-driven framework that extracts *unique features* from the tails of the signal distribution which has the ability to isolate, even without expert knowledge, neonates with seizures. Our contributions thus pave the way for efficient representation learning of extremes, which can be useful in a wide range of scientific applications.

Many brain-state analyses involve extraction of features through dependence matrices (Tononi et al., 1998; Goutte et al., 2001; Liu et al., 2012). In fact, a number of studies demonstrated associations between physiological signals (through brain functional connectivity), and behavior and cognition (Han et al., 2013; Donofry et al., 2020; Shapson-Coe et al., 2024). In addition to the spectral density matrix (see Ch. 4 of Shumway and Stoffer, 2000), canonical coherence—introduced by Brillinger (1969) as the time-series analogue of canonical correlation (Hotelling, 1936)—provides a multivariate measure of synchrony between two groups of signals at specific frequencies. Extending this framework to frequency bands (defined in Section 2.2) in the presence of outlying observations, the Kendall’s tau based canonical coherence (Talentó et al., 2024) provides a rank-based estimator for the canonical coherence of filtered signals, enabling discrimination of brain states that is robust to outliers. However, there are cases when connectivity in the bulk of the data differs from connectivity at the tails. As demonstrated in Talentó et al. (2025), there are key features of extreme events that are only highlighted when focus is placed on the joint tails of brain signals. This is true for brain connectivity, where many extreme neurological events, such as seizures, are a result of concurrent or interrelated extreme firing of neurons (NIH, 2023). This complexity has led to recent growing interest in multivariate risk analysis in neuroscience applications (Guerrero et al., 2023; Redondo et al., 2025; Talentó et al., 2025; McGonigle

et al., 2025), which addresses questions such as “What is the likelihood that two brain signals exhibit extreme amplitudes simultaneously?”

The extremal dependence measure (EDM), introduced in Resnick (2004) and studied by Larsson and Resnick (2012), encodes tail dependence via the framework of multivariate regular variation (Resnick, 2007). Cooley and Thibaud (2019) extended the EDM beyond the bivariate setting by introducing the tail pairwise dependence matrix (TPDM), which, analogous to a covariance matrix, encodes extremal dependence for random vectors. The TPDM has established the basis for a number of multivariate analyses in extreme value theory, such as high-dimensional graphical or causal analysis (Jiang et al., 2020; Gong et al., 2024; Jiang et al., 2025b) and clustering (Richards et al., 2025; Elsom and Pawley, 2025). In this paper, we utilize the TPDM to propose a novel measure of canonical tail dependence (CTD) to discriminate the joint-tail regional structure of neonates with extreme brain conditions (e.g., seizures) from those patients with normal brain conditions (e.g., seizure-free). We define CTD as the maximized EDM value between linear combinations of signals from two brain regions. Using these optimized linear combinations, we can further investigate patterns associated with different brain conditions based on the tail connectivity of the signals.

A number of studies consider features extracted from multivariate extremes for hard clustering based on, e.g., max-linear models, hidden regular variation, max-stable processes, and conditional limit laws (Janßen and Wan, 2020; Meyer and Wintenberger, 2024; Guerrero et al., 2022; O’Toole et al., 2025). However, extending these hard clustering approaches to multi-subject EEG data is non-trivial. EEG signals display complex and non-stationary cross-dependencies (Redondo et al., 2025; Ombao and Pinto, 2024), high noise levels, and significant inter-subject variability (Ma et al., 2025b). Thus, relying on a single ‘hard’ cluster in combination with standard feature-extraction techniques frequently fails to represent a subject’s behavior accurately (Seghier et al., 2007). This leads us to develop a novel mechanism for feature extraction from the joint-tails of brain signals and propose an accurate soft clustering framework for multivariate extremes. Our method provides a membership degree to each subject based on their extremal brain connectivity structure.

One well-known soft clustering technique is fuzzy clustering, grounded in Zadeh’s fuzzy set theory (Zadeh et al., 1996), which treats partitions between units as continuous transitions rather than hard boundaries. The most widely-used approach is the Fuzzy C-Means (FCM) algorithm (Bezdek et al., 1984) which has gained popularity in applications that include image (Wang and Bu, 2010;

Huang et al., 2019) and signal processing (Murugappan et al., 2007; Zheng et al., 2013; Zhang et al., 2021). There are recent developments in soft clustering of multivariate signals that are quantile-based (López-Oriona et al., 2022), and Ma et al. (2025a) showed that canonical coherence-based fuzzy clustering is superior to the state-of-the-art fuzzy clustering, namely, traditional FCM, variable-based principal component analysis (PCA) clustering (He and Tan, 2018), quantile cross-spectral density based fuzzy clustering (López-Oriona et al., 2022), wavelet-based clustering (D’Urso and Maharaj, 2012), and fuzzy clustering using PCA (Ma et al., 2025b). Hence, we apply canonical correlation based soft clustering on seizure data of neonates and presented the result in Section 2. From our preliminary analyses, traditional canonical correlation based soft clustering do not adequately separate seizure vs non-seizure patients. This is because these clustering methods focus on the bulk of the distribution and are not tailored to extreme events. While D’Urso et al. (2017) proposed a fuzzy clustering of extremes, this is only for univariate time series, and not multivariate brain signals.

In summary, our paper provides two key innovations: (1) a novel tail dependence measure (the CTD) between random vectors, which facilitates representation learning of extremal connectivity structure; and (2) an unsupervised soft clustering method for multivariate extremes, applied to identification of neonates with seizures. Our goal is to provide explainable features that reveal key information contained in the tail of the joint distribution. Thus, one of the major advantages of our method is its interpretability; our method offers a pathway to relate soft clusters and tail dependence of brain signals. Through the CTD, we can visualize the unifying characteristics of each cluster, facilitating accurate differentiation between neonates with and without seizures. Although applied to brain signals, our method is applicable in other fields, such as finance and environmental science.

The remainder of the article is organized as follows. Section 2 introduces the neonatal seizure data and an exploratory soft clustering based on classical canonical correlation. Section 3 details background on multivariate regular variation, presents our novel canonical tail dependence (CTD) measure, and provides our algorithm for fuzzy clustering. Section 4 provides results from a simulation study. Section 5 reports the novel findings of our application clustering patients in a neonatal intensive care unit through their electroencephalogram recordings. Finally, Section 6 summarizes the study and discusses limitations of the proposed method.

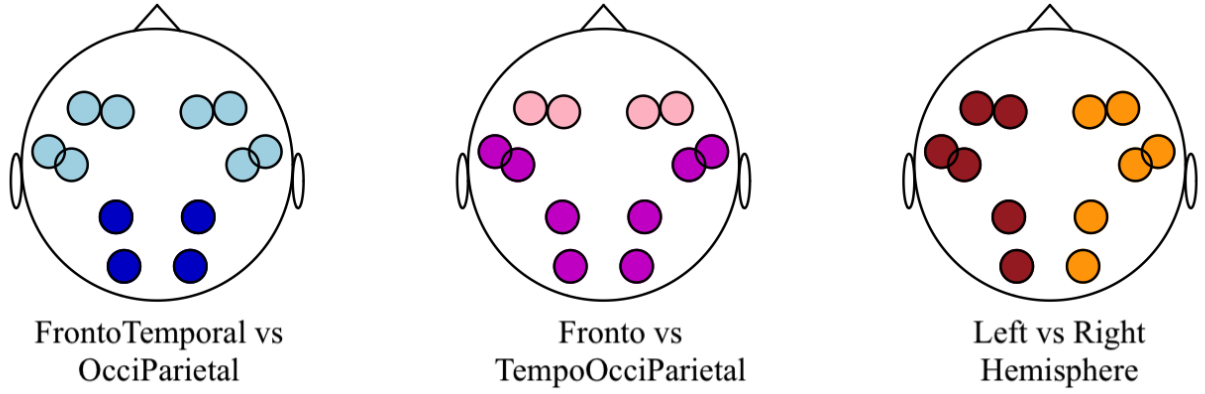


Figure 1: EEG channel locations on the scalp of different regions of interests: FrontoTemporal (light blue nodes) vs OcciParietal (dark blue nodes), Frontal (light pink nodes) vs TempoOcciParietal (dark pink nodes), and left (brown nodes) vs right hemisphere (orange nodes).

2 The Neonatal Electroencephalography Data

In this section, we first introduce the dataset (Section 2.1) and then describe the EEG preprocessing steps used to address the spectral-domain analysis problem (Section 2.2). In Section 2.3, we present a brief exploratory analysis using canonical-correlation-based feature extraction.

2.1 Data

The data are available at <https://zenodo.org/records/2547147> and the EEG signals were recorded from neonates admitted to an intensive care unit in Finland (Stevenson et al., 2019). These signals were recorded at 19 electrodes covering the entire scalp. Seizure occurrence labels are based on expert annotations. We follow the preprocessing pipeline of Talento et al. (2025): selecting electrodes with consistent quality across subjects, followed by application of the Early Stage Pre-processing (PREP) pipeline (see Bigdely-Shamlo et al., 2015, for details). PREP is chosen over alternative artifact detection methods as it preserves extremal behavior. Subjects with an excessive proportion of suspiciously small values in the cleaned EEG are excluded. The analysis includes $N = 14$ subjects: six non-epileptic subjects and eight epileptic subjects with seizures primarily localized in the right hemisphere of their brain.

We seek to discern seizure-free neonates vs neonates who had primary localization of seizure at the right hemisphere. To do this, two groups of channels associated with seizure activity were identified, denoted as $X \in \mathbb{R}^P$ and $Y \in \mathbb{R}^Q$ (defined more formally in Equation (3)). Three forms of region-to-region connectivity based on $D = P + Q = 12$ channels are of interest in our analysis, namely:

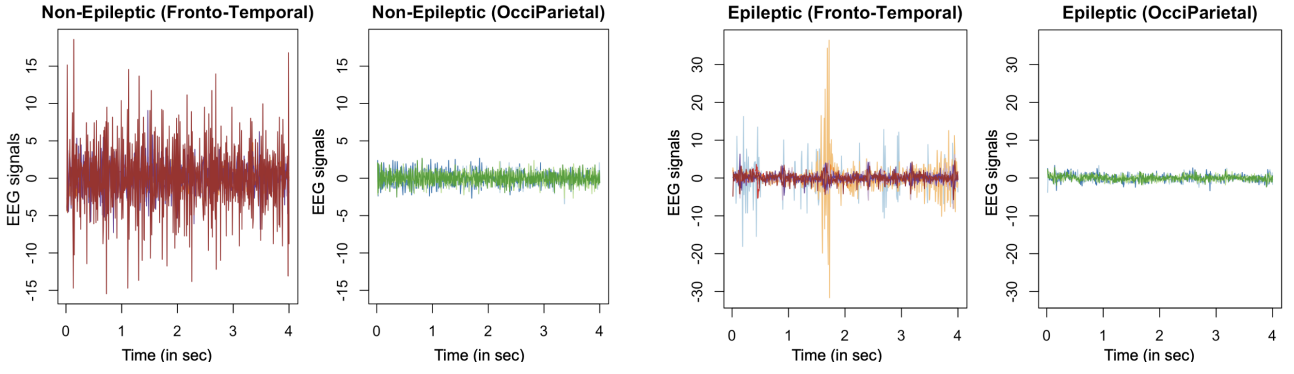


Figure 2: Detrended EEG signals from FrontoTemporal lobe (1st and 3rd panels) and OcciParietal lobe (2nd and 4th panels) of non-epileptic patient (1st and 2nd panels) and epileptic patient (3rd and 4th panels).

(i) FrontoTemporal-vs-OcciParietal (FT-OP): (F3, F7, F4, F8, T3, T4, T5, T6) vs (P3, P4, O1, O2) i.e., $P = 8$ and $Q = 4$. Most primary localizations in the subjects arise from the OcciParietal lobe; thus, isolating these channels provides a more informative spatial configuration for our analysis. Moreover, literature highlights the temporal lobe as the most common focal point of seizures ([Pisani et al., 2021](#)). See blue colored nodes in Figure 1 (left panel).

(ii) Fronto-vs-TempoOcciParietal (F-TOP): (F3, F7, F4, F8) vs (T3, T4, T5, T6, P3, P4, O1, O2) i.e., $P = 4$ and $Q = 8$. The frontal lobe is known to play a role in motor behavior in neonates, which may be disrupted by seizures ([Panayiotopoulos, 2005](#)). Hence, we tested the partitioning frontal lobe from all other lobes. See pink colored nodes in Figure 1 (middle panel).

(iii) Left-vs-Right Hemisphere: (F3, F7, T3, T5, P3, O1) vs (F4, F8, T4, T6, P4, O2) i.e., $P = 6$ and $Q = 6$. As the primary localization of the seizures are in the right hemisphere, we also explore the connectivity between the left and right hemispheres. See orange and brown colored nodes in Figure 1 (right panel).

Figure 2 shows sample signals taken from a non-epileptic and epileptic patients. From here, we can see that FrontoTemporal channels (1st and 3rd panels) are heavy-tailed for both epileptic and non-epileptic patients. However, the tail behavior seems different. The goal of our paper, then, is to provide a practical feature extraction tool for examining potential discrepancies in tail behavior across brain conditions.

2.2 Spectral Domain Features

Analyzing brain signals during high-frequency oscillations offers information on bursts of its electrical activity, e.g., seizures (Guerrero et al., 2023; Pinto-Orellana and Lopour, 2024). We thus extract features from the EEGs that are attributed to the standard frequency bands: delta, for $\Omega = (0 - 4]\text{Hz}$; theta, for $\Omega = (4 - 8]\text{Hz}$; alpha, for $\Omega = (8 - 12]\text{Hz}$; beta, for $\Omega = (12 - 30]\text{Hz}$; gamma, for $\Omega = (30 - 50]\text{Hz}$.

Our approach is to divide the EEG recording into B disjoint blocks where each block contains A number of time points. For block b , denote the local discrete Fourier transform (DFT) of the j -th channel at the fundamental frequency $\omega_a := a/A$, $a = 0, 1, \dots, A - 1$, as

$$d_{j,b}(\omega_a) = \frac{1}{\sqrt{A}} \sum_{t=A(b-1)+1}^{A(b-1)+A} E_{j,t} \exp(-i2\pi\omega_a t), \text{ for } j = 1, \dots, D,$$

where $-i = \sqrt{-1}$ and $E_t \in \mathbb{R}^D$ denotes the EEG signals observed at time t , $t = 1, 2, \dots, AB$, that is ‘locally stationary’: the time series is approximately stationary on each of the B time blocks. Then, we compute the local periodogram (at block b and frequency ω_a),

$$Z_{j,b}(\omega_a) = |d_{j,b}(\omega_a)|^2 = \frac{1}{A} \left| \sum_{t=A(b-1)+1}^{A(b-1)+A} E_{j,t} \exp(-i2\pi\omega_a t) \right|^2.$$

The local periodogram $Z_{j,b}(\omega_a)$ measures the contribution of the amplitude of the oscillation at frequency ω_a to the total variance. Consistent with standard analyses of brain signals (Srinivasan, 2007), we aggregate the local periodogram over the standard frequency bands. Hence, the local Ω -periodogram for channel $j = 1, \dots, D$, at time-block b , is

$$Z_{j,b}(\Omega) = \frac{1}{|\Omega|} \sum_{\{a: \text{SR} \times \omega_a \in \Omega\}} Z_{j,b}(\omega_a), \quad (1)$$

where SR is the sampling rate. In our application, the sampling rate is $\text{SR} = 256\text{Hz}$ and the local time window is two seconds; hence, $A = 256 \times 2 = 512$.

2.3 Canonical correlation based soft clustering

Canonical correlation analysis (CCA) finds the maximum linear association among all possible linear combinations of the columns of two matrices. Let $X \in \mathbb{R}^P$ and $Y \in \mathbb{R}^Q$. The CCA finds the vectors

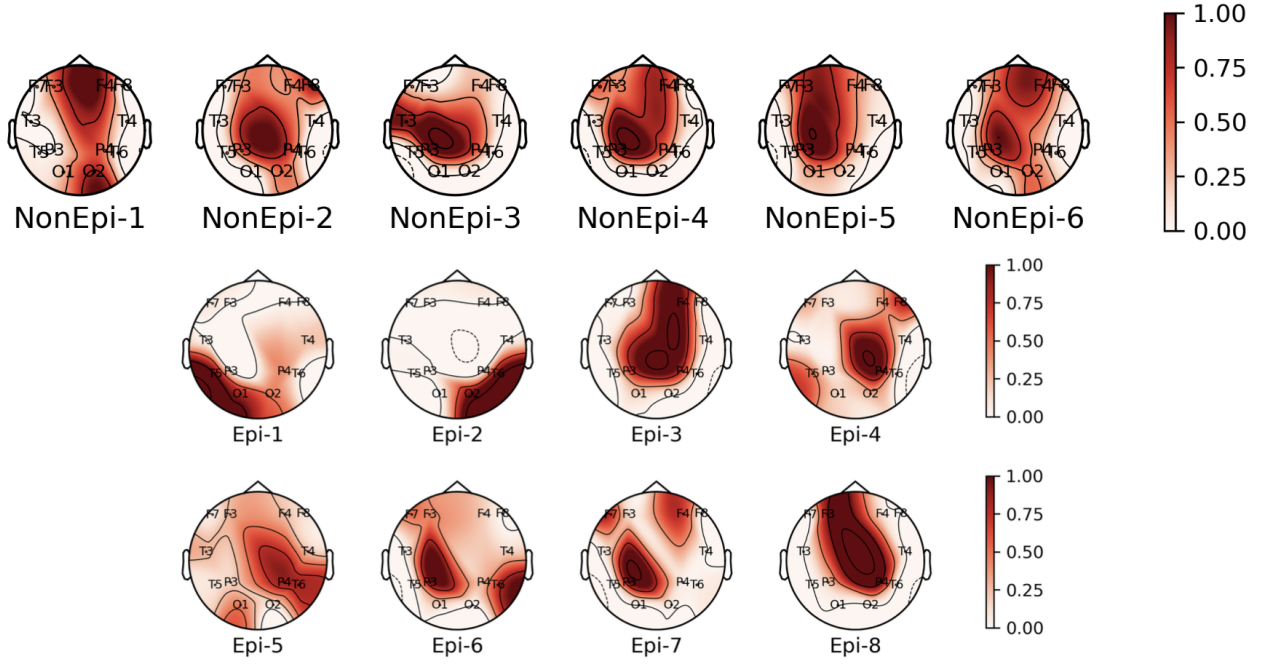


Figure 3: Tomomaps (using mne Python package, see [Gürsoy et al., 2014](#)) of $|\hat{\Lambda}_0^{(n)}|$, at the gamma band for FrontoTemporal-vs-OcciParietal connectivity. Canonical vectors of six non-epileptic neonates (first row) and eight epileptic neonates (second and third row) with primary localization on *right hemisphere*. Darker color represents higher eigenvector magnitude for channels $j = 1, \dots, 12$, labeled F3, F7, F4, F8, T3, T4, T5, T6, P3, P4, O1, O2.

$\gamma_0 \in \mathbb{R}^P$ and $\beta_0 \in \mathbb{R}^Q$ that maximize the correlation between $\gamma_0^\top X$ and $\beta_0^\top Y$. These vectors are called “canonical directions” or “canonical variates”; and the corresponding correlation is the “canonical correlation”. Precisely, the canonical correlation is defined by [Hotelling \(1936\)](#) as

$$\rho = \max_{\gamma_0, \beta_0} \text{Cor}(\gamma_0^\top X, \beta_0^\top Y)^2 \in (0, 1),$$

subject to the constraint $\gamma_0^\top \text{Cov}(X, X) \gamma_0 = \beta_0^\top \text{Cov}(Y, Y) \beta_0 = 1$ for identifiability.

Define $Z_b^{(n)} = (X_b^{(n)\top}, Y_b^{(n)\top})^\top$ as the concatenated vector of $X_b \in \mathbb{R}^P$ and $Y_b \in \mathbb{R}^Q$, for $b = 1, \dots, B$ blocks and $n = 1, \dots, N$ subjects. For notational simplicity, we omit Ω in Equation (1), as the analyses are carried out separately for each frequency band. For $N = 14$, we obtain estimates of $\Lambda_0^{(n)} := (\gamma_0^{(n)\top}, \beta_0^{(n)\top})^\top \in \mathbb{R}^{P+Q}$, through the estimation procedure provided in Chapter 10 of [Mardia and Kent \(1979\)](#). We apply the fuzzy C-means algorithm to absolute values of $\Lambda_0 := (\Lambda_0^{(1)}, \dots, \Lambda_0^{(N)})^\top \in \mathbb{R}_+^{N \times D}$, where $D = P + Q$, with two clusters (to identify epileptic and non-epileptic subjects). Here, we use m to indicate the degree of fuzziness, with higher values of m producing softer clustering assignments. A more formal definition of m is to be provided in Section 3.3.

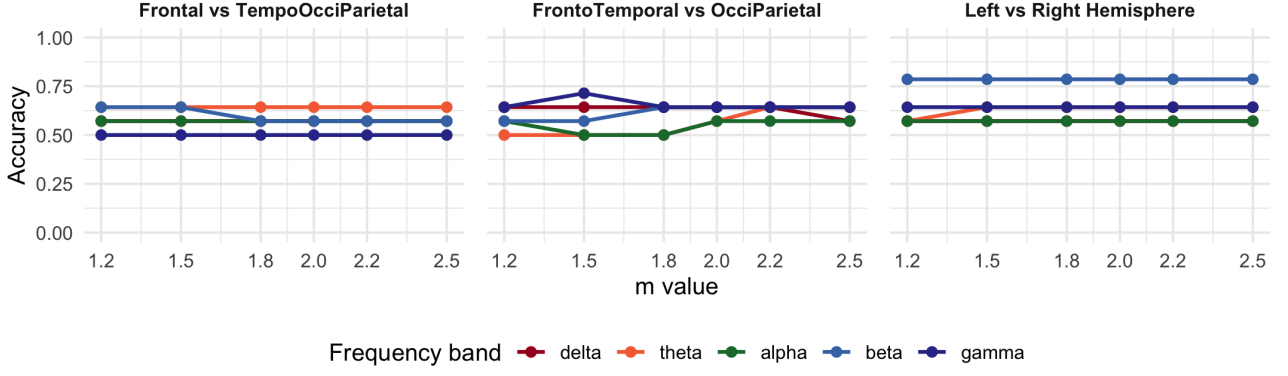


Figure 4: Accuracy of CCA-based fuzzy clustering evaluated for different values of fuzzy parameter m and for all frequency bands (i.e., delta, theta, alpha, beta and gamma). Colors differ with frequency band and the regions of interest differ across panels.

We display (smoothed) estimates of $|\Lambda_0|$ for FrontoTemporal-vs-OcciParietal connectivity in Figure 3, i.e., $|\Lambda_0| \in \mathbb{R}_+^{14 \times 12}$. From this figure, it is unclear how the connectivity structure of the spectral features (i.e., periodogram) changes for different clusters. Figure 4 provides the clustering accuracy (see Equation (9) below for its exact definition) of the CCA-based clustering procedure for different levels of m , different frequency bands and the three regional connectivities. The limitation of the standard CCA is that the accuracy is not sufficiently high (under 80%) to distinguish epileptic and non-epileptic subjects. This is a major weakness and is a motivation to develop a feature extracting mechanism tailored to extreme events. In the next section, we develop a novel method for the joint tails of the distribution using multivariate extreme value theory. Our method provides a principled way of extracting connectivity-based features from the tails of the distribution to offer an interpretable and accurate way of clustering brain signals.

3 The Proposed Methodology

We detail the multivariate regular-variation framework in Section 3.1, and then introduce our novel canonical tail dependence (CTD) measure in Section 3.2. This is followed by our proposed fuzzy extremal clustering algorithm in Section 3.3.

3.1 Background: Multivariate Regular Variation

A well-established representation of joint tail behavior is multivariate regular variation (Resnick, 2007). We follow Cooley (2025) in its definition.

Definition 3.1. (Multivariate Regular Variation, [Cooley, 2025](#))

A P -dimensional random vector, X , is ‘regularly varying’ of order $\alpha > 0$, i.e., $X \in \text{RV}^P(\alpha)$, if there exists a normalizing sequence $w(u) \rightarrow \infty$ such that

$$w(u)\mathbb{P}(u^{-1}X \in C) \xrightarrow{v} \nu_X(C), \quad u \rightarrow \infty,$$

where $\nu_X(\cdot) \in [-\infty, \infty]^P \setminus \{0_P\} := \overline{\mathbb{R}}^P$ is a limiting measure on the space of (non-trivial) Radon measures for Borel sets $C \in [-\infty, \infty]^P \setminus \{0_P\}$, and \xrightarrow{v} denotes ‘vague’ convergence of measures. The limit measure is $(-\alpha)$ -homogeneous, i.e., $\nu_X(zC) = z^{-\alpha}\nu_X(C)$, and the normalizing sequence satisfies $\lim_{u \rightarrow \infty} w(uz)/w(u) = z^\alpha$, for $z > 0$.

Following [Cooley and Thibaud \(2019\)](#), we set $\alpha = 2$. This is without loss of generality (with respect to marginal transformations) as we can always standardize the data to have $\text{RV}^1(2)$ margins (see, e.g., [Jiang et al., 2025a](#)). The homogeneity of the limit measure, $\nu_X(\cdot)$, makes a radial-angular representation particularly well-suited for describing multivariate regular variation. Let $(R, \psi) := (\|x\|, x/\|x\|)$ be the vector of radial and angular components where $\|\cdot\|$ is the L_2 norm. For large $r > 0$, define the set

$$C(r, \Psi) := \{x \in \overline{\mathbb{R}}^P : R > r, \psi \in \Psi\}, \quad (2)$$

where $\Psi \subset \mathbb{S}^{P-1}$, with $\mathbb{S}^{P-1} := \{x \in \mathbb{R}^P : \|x\| = 1\}$ the unit $(P-1)$ -sphere. We then define the *angular measure* as $H_X(\Psi) := \nu_X(C(1, \Psi))$, which allows us to quantify the relative contribution of components of X to multivariate extreme events ([Cooley, 2025](#)). In other words, H_X can quantify the strength of extremal association between variables through ψ (see [Resnick, 2007](#), for details). [Resnick \(2004\)](#) provide a summary measure of pairwise extremal association by defining the extremal dependence measure (EDM) of a vector $(X_1, X_2)^\top \in \text{RV}^2(2)$ as

$$\sigma(X_1, X_2) = \int_{\mathbb{S}^1} \psi_1 \psi_2 dH_{(X_1, X_2)}(\psi) = 2 \lim_{r \rightarrow \infty} \mathbb{E}(\psi_1 \psi_2 | R > r) \in [0, 1],$$

where the strength of extremal dependence in $(X_1, X_2)^\top$ increases with σ . [Cooley and Thibaud \(2019\)](#) proposed the tail pairwise dependence matrix (TPDM) which extends the EDM to a $P \times P$ matrix. We

denote the TPDM by $\Gamma \in \mathbb{R}^{P \times P}$ and its elements are given by the following formula:

$$\Gamma_{jk} := \int_{\mathbb{S}^{P-1}} \psi_j \psi_k dH_X(\psi) = P \lim_{r \rightarrow \infty} \mathbb{E}(\psi_j \psi_k | R > r)$$

for $j, k = 1, \dots, P$, where now the radius R and the angles ψ_j, ψ_k are computed based on the full random vector $X \in \mathbb{R}^P$. Furthermore, note that (a) the TPDM evaluates the integral over the entire set \mathbb{S}^{P-1} , in contrast to the set \mathbb{S}^1 used in the EDM, and (b) the TPDM is a positive semi-definite and symmetric matrix.

3.2 Canonical Tail Dependence

Consider now a D -dimensional regularly varying vector $Z \in \text{RV}^D(2)$. Suppose that Z is composed of two distinct subsets, so that $Z = (X^\top, Y^\top)^\top$, where $X \in \text{RV}^P(2)$ represents features from one brain region, and $Y \in \text{RV}^Q(2)$ represents features from a second brain region, and $D = (P + Q)$ with $P, Q \geq 2$. We summarize extremes in each brain region using vectors $\gamma \in \mathbb{R}^P$ and $\beta \in \mathbb{R}^Q$. Let $\gamma^\top X \in \mathbb{R}$ and $\beta^\top Y \in \mathbb{R}$ be the projections of X and Y onto the line defined by vectors γ and β for brain regions one and two, respectively. The canonical tail-dependence is the squared maximal EDM between the projections of the two brain regions.

Definition 3.2. Let $X \in \text{RV}^P(2)$, $Y \in \text{RV}^Q(2)$, $\gamma \in \mathbb{R}^P$, and $\beta \in \mathbb{R}^Q$. The “canonical tail dependence” (CTD) is

$$\tau = \max_{\gamma, \beta} \left\{ \sigma \left(\gamma^\top X, \beta^\top Y \right) \right\}^2 \in [0, 1]. \quad (3)$$

The canonical tail dependence, τ , generalizes the approach in [Russell et al. \(2016\)](#), which regresses multiple extreme covariates on a single dependent variable. With the CTD, our goal is to identify linear combinations of two sets of variables that maximize tail dependence. Direct numerical maximization of this objective function, however, incurs a substantial computational cost, particularly for large P and Q . To drastically simplify computations, we derive an analytical solution to Equation (3) using the tail pairwise-dependence matrix (TPDM).

Proposition 3.1. Let $Z = (X^\top, Y^\top)^\top$ where $X \in \text{RV}^P(2)$ and $Y \in \text{RV}^Q(2)$. Define $\Gamma_{XX} \in \mathbb{R}^{P \times P}$ and $\Gamma_{YY} \in \mathbb{R}^{Q \times Q}$ to be the TPDMs of X and Y , respectively. Moreover, let $\Gamma_{XY} = \Gamma_{YX}^\top \in \mathbb{R}^{P \times Q}$ be the

cross-TPDM between X and Y . The TPDM of Z has the block matrix form

$$\Gamma = \begin{pmatrix} \Gamma_{XX} & \Gamma_{XY} \\ \Gamma_{YX} & \Gamma_{YY} \end{pmatrix}.$$

The CTD in Equation (3) is equivalent to

$$\tau = \max_{\substack{\gamma, \beta: \\ \gamma^\top \Gamma_{XX} \gamma = \beta^\top \Gamma_{YY} \beta = 1}} \{\gamma^\top \Gamma_{XY} \beta\}^2,$$

Proof. The proof of this proposition takes advantage of the linearity of the EDM (Proposition 1, Cooley, 2025). We show that $\sigma(\gamma^\top X, \beta^\top Y) = \gamma^\top \Gamma_{XY} \beta$. Define $\zeta : \mathbb{R}^{P+Q} \rightarrow \mathbb{R}^2$ as the function

$$\zeta(Z) = (\gamma^\top X, \beta^\top Y) := Z_\zeta.$$

We then define the *canonical angles* ψ_ζ (similarly to Equation (2)) as

$$\psi_\zeta := (\psi_{\zeta,1}, \psi_{\zeta,2})^\top = Z_\zeta / \|Z_\zeta\| \in \Psi_\zeta \subset \mathbb{S}^1,$$

which can be linked backed to the angles ψ of Z through the transformation $\psi_\zeta := \zeta(\psi) / \|\zeta(\psi)\|$. Further, let $\zeta^{-1}(\Psi_\zeta) := \{\psi \in \mathbb{S}^{D-1} : \zeta(\psi) / \|\zeta(\psi)\| \in \Psi_\zeta\}$. Following Cooley (2025), the limit measure of Z can be rewritten in terms of the conditional set

$$C(1, \Psi_\zeta) := \{Z \in \mathbb{R}^D : \|\zeta(\psi)\| > 1, \zeta(\psi) / \|\zeta(\psi)\| \in \Psi_\zeta\},$$

which depends only on the linear combination, Z_ζ . Hence, the angular measure H_{Z_ζ} of Z_ζ is now given as

$$\begin{aligned} \nu_Z(C(1, \Psi_\zeta)) &= \int_{\zeta^{-1}(\Psi_\zeta)} \int_{1/\|\zeta(\psi)\|}^{\infty} \alpha r^{-\alpha-1} dr dH_Z(\psi) \\ &= \int_{\zeta^{-1}(\Psi_\zeta)} \|\zeta(\psi)\|^\alpha dH_Z(\psi) =: H_{Z_\zeta}(\psi_\zeta). \end{aligned} \quad (4)$$

We partition the set $\{\psi \in \mathbb{S}^{D-1} : \zeta(\psi) / \|\zeta(\psi)\| \in \Psi_\zeta\}$ to correspond with the indices of X and Y , i.e., $\psi := (\psi_X^\top, \psi_Y^\top)^\top$. Hence, by this definition and $\alpha = 2$, we have

$$\begin{aligned}
\sigma(\gamma^\top X, \beta^\top Y) &= \int_{\mathbb{S}^1} \psi_{1,\zeta} \psi_{2,\zeta} dH_\zeta(\psi_\zeta) \\
&= \int_{\mathbb{S}^{D-1}} \frac{\gamma^\top \psi_X}{\|\zeta(\psi)\|} \frac{\beta^\top \psi_Y}{\|\zeta(\psi)\|} \|\zeta(\psi)\|^2 dH_Z(\psi) \\
&= \int_{\mathbb{S}^{D-1}} (\gamma_1 \psi_1 + \dots + \gamma_P \psi_P) (\beta_1 \psi_{P+1} + \dots + \beta_Q \psi_D) dH_Z(\psi) \\
&= \gamma_1 \int_{\mathbb{S}^{D-1}} \psi_1 \psi_{P+1} dH_Z(\psi) \beta_1 + \dots + \gamma_P \int_{\mathbb{S}^{D-1}} \psi_P \psi_D dH_Z(\psi) \beta_Q \\
&= \gamma_1 \Gamma_{1,P+1} \beta_1 + \dots + \gamma_P \Gamma_{P,D} \beta_Q \\
&= \gamma^\top \Gamma_{XY} \beta,
\end{aligned}$$

where the second line follows from Equation (4) and the transformation $\psi_\zeta := \zeta(\psi)/\|\zeta(\psi)\|$. Note that the surface Jacobian of this transformation is equal to one. \square

Proposition 3.1 gives a straightforward estimator of the CTD. After estimating the TPDM, Γ , we solve the optimization problem in Equation (3) through Proposition 3.1, i.e., the optimization of CTD reduces to an eigen-decomposition problem similar to Theorem 10.2.1 in Mardia and Kent (1979). We then employ this optimization problem to characterize a novel connectivity structure in the joint extremes of two vectors, which we call “canonical tail variates” (defined below).

Definition 3.3. Let $X \in RV^P(2)$, $Y \in RV^Q(2)$, $\gamma \in \mathbb{R}^P$, and $\beta \in \mathbb{R}^Q$. Further, let $\Gamma_{XX} \in \mathbb{R}^{P \times P}$ and $\Gamma_{YY} \in \mathbb{R}^{Q \times Q}$ be the TPDMs of X and Y , respectively. The “canonical tail-variates”, denoted by γ^*, β^* , are defined as

$$\gamma^*, \beta^* = \arg \max_{\gamma, \beta} \left\{ \sigma(\gamma^\top X, \beta^\top Y) \right\}^2, \quad (5)$$

subject to the constraint $\gamma^\top \Gamma_{XX} \gamma = \beta^\top \Gamma_{YY} \beta = 1$ for identifiability. Furthermore, the “extremal scores” are defined as $\gamma^{*\top} X$ and $\beta^{*\top} Y$.

From Definition 3.3 and Proposition 3.1, it follows that the canonical tail-variates can be computed as

$$\gamma^*, \beta^* = \arg \max_{\substack{\gamma, \beta: \\ \gamma^\top \Gamma_{XX} \gamma = \beta^\top \Gamma_{YY} \beta = 1}} \{ \gamma^\top \Gamma_{XY} \beta \}^2.$$

Theorem 10.2.1 in Mardia and Kent (1979) further implies that τ is the first eigenvalue of

$$G_1 = \Gamma_{XX}^{-1} \Gamma_{XY} \Gamma_{YY}^{-1} \Gamma_{YX} \text{ or, equivalently, of } G_2 = \Gamma_{YY}^{-1} \Gamma_{YX} \Gamma_{XX}^{-1} \Gamma_{XY}. \quad (6)$$

Moreover, the eigenvectors that correspond to the largest eigenvalues of $G_1 \in \mathbb{R}^{P \times P}$ and $G_2 \in \mathbb{R}^{Q \times Q}$ are defined, respectively, as

$$\lambda_1 := \Gamma_{XX}^{1/2} \gamma^* \in \mathbb{R}^P \text{ and } \lambda_2 := \Gamma_{YY}^{1/2} \beta^* \in \mathbb{R}^Q, \quad (7)$$

which we refer to as the “tail-topology”. The absolute value of our tail-topology reflects the contribution of each component in attaining maximum tail dependence between two random vectors. In applications to brain signals, the tail-topology captures the weights assigned to each channel that drive the two brain regions to produce high amplitudes simultaneously.

3.3 Fuzzy Clustering of Multivariate Extremes

We now develop a fuzzy clustering algorithm based on CTD. One novel feature of our method is that it uses the first eigenvectors (that correspond to the largest eigenvalues), λ_1 and λ_2 , of the canonical tail-dependence (as defined in Equation (7)) to represent the topology of multivariate extremes. Suppose we have N subjects, each with D -variate data $Z_b^{(n)} \in \text{RV}^D(2)$, for $n = 1, \dots, N$, and time block $b = 1, \dots, B$. We now provide a step-by-step procedure for Fuzzy Clustering of Multivariate Extremes via the CTD.

Step 1: Estimate the CTD. We follow [Cooley and Thibaud \(2019\)](#) for estimating the TPDM. For each subject data $\{Z_b^{(n)}\}_{b=1}^B$, $n = 1, \dots, N$, estimate the elements of the TPDM, denoted by $\Gamma^{(n)} \in \mathbb{R}^{D \times D}$, by

$$\hat{\Gamma}_{jk}^{(n)} = \frac{D}{c} \sum_{b=1}^B \frac{Z_{j,b}^{(n)} Z_{k,b}^{(n)}}{\{\|Z_b^{(n)}\|\}^2} \mathbb{I}\{\|Z_b^{(n)}\| > r_n\}, \quad (8)$$

for $j, k = 1, \dots, D$, where $\mathbb{I}\{\cdot\}$ is the indicator function, $c = \sum_{b=1}^B \mathbb{I}\{\|Z_b^{(n)}\| > r_n\}$ is the number of radial exceedances above the threshold $r_n > 0$ and $\|\cdot\|$ is the L_2 norm. Hereafter, we take r_n as the empirical q -th quantile, i.e.,

$$r_n := \hat{F}_{\|Z_b^{(n)}\|}^{-1}(q)$$

where $\hat{F}_{\|Z_b^{(n)}\|}(q)$ is the empirical distribution function of $\{\|Z_b^{(n)}\|\}_{b=1}^B$ and $q \in (0, 1)$ is a probability level close to one. We advocate conducting a sensitivity analysis to choose the value of r_n , $n = 1, \dots, N$. Using $\hat{\Gamma}^{(n)}$, we obtain estimates of the tail topology, $\hat{\lambda}_1^{(n)}$ and $\hat{\lambda}_2^{(n)}$, through the eigen-decomposition in Equation (6).

Step 2: Stack the tail-connectivity features. Here, we take the absolute tail-topologies. [Lucińska \(2014\)](#) showed that taking the absolute values of eigenvectors stabilizes clustering assignment and avoids ambiguity brought by the signs of the vectors. Denote the set of absolute CTD eigenvectors of $\{Z_b^{(n)}\}_{b=1}^B$ to be

$$\Lambda_n = \left(|\hat{\lambda}_1^{(n)\top}|, |\hat{\lambda}_2^{(n)\top}| \right)^\top \in [0, \infty)^D,$$

for $n = 1, \dots, N$. Hence, for N subjects, we have $\Lambda = \{\Lambda_1, \dots, \Lambda_N\} \in [0, \infty)^{D \times N}$ as the collection of tail-topology features.

Step 3: Fuzzy clustering and computation of the membership matrix. We then perform a fuzzy C -means clustering (FCM) based on Λ . FCM involves solving for a set of $S \in \mathbb{N}$ cluster centers $\bar{\Lambda} = \{\bar{\Lambda}_1, \dots, \bar{\Lambda}_S\} \in [0, \infty)^S$, and the fuzzy coefficient matrix, denoted as $U \in [0, 1]^{N \times S}$. The elements of the fuzzy coefficient matrix, U_{ns} , quantify the membership degree for subject n to cluster $s \in \{1, \dots, S\}$. The FCM method finds $\bar{\Lambda}$ and U by solving the minimization problem:

$$\min_{\bar{\Lambda}, U} \sum_{n=1}^N \sum_{s=1}^S (U_{ns})^m \|\Lambda_n - \bar{\Lambda}_s\|^2, \text{ subject to } \sum_{s=1}^S U_{ns} = 1, U_{ns} \geq 0, \forall n = 1, \dots, N,$$

where $m \in (1, 3)$ is the fuzziness parameter that governs the extent of cluster overlap in the partition. This optimization problem is solved via an iterative procedure, i.e., we update the current values of U using

$$U_{ns} = \left(\sum_{s' \in \{1, \dots, S\} \setminus s} \left(\frac{\|\Lambda_n - \bar{\Lambda}_s\|^2}{\|\Lambda_n - \bar{\Lambda}_{(s')}\|^2} \right)^{\frac{1}{m-1}} \right)^{-1},$$

where $s' \neq s$. For the centers, we update them according to

$$\bar{\Lambda}_s = \frac{W(m)\Lambda_n}{W(m)}, \text{ where } W(m) = \sum_{n=1}^N (U_{ns})^m.$$

Step 4: Label assignment. Using the estimated membership matrix U , assign a label to each subject $n = 1, \dots, N$ by selecting a cut-off. In this paper, if $U_{ns} > 0.7$, we assign subject n to cluster s . If $U_{ns} < 0.7$ for all $s = 1, \dots, S$, then the subject is declared as a fuzzy-subject, i.e., the subject has tail characteristics that are compatible with more than one cluster.

For data-driven selection of S , we could exploit a number of cluster validity indices, e.g., the fuzzy silhouette index from [Rawashdeh and Ralescu \(2012\)](#). In our application, we set $S = 2$, in order to identify groups of neonates who have had seizure. We use experts' annotations as the true cluster labels

and create a confusion matrix, $M \in \{0, \dots, N\}^{2 \times 2}$, to measure accuracy. The rows of M are the experts' labels and the columns are the estimated cluster labels. We calculate the accuracy as

$$\text{Accuracy} = \frac{\max\{M_{11} + M_{22}, M_{12} + M_{21}\}}{N} \in [0.5, 1]. \quad (9)$$

We perform the clustering for different values of m in the interval $(1, 3)$ and select the m that gives the highest accuracy.

4 Simulation

In this section, we present simulation results under various settings comparing our fuzzy extremal clustering algorithm with the classical fuzzy C-means algorithm.

4.1 Simulation Settings

We demonstrate the accuracy of the fuzzy extremal clustering algorithm with multivariate regularly varying random vectors. To simulate multivariate regularly varying vectors, we follow the simulation method of [Gong et al. \(2024\)](#), which is based on the framework of [Cooley and Thibaud \(2019\)](#).

Let $Z_b^{(n)} := (X_b^{(n)\top}, Y_b^{(n)\top})^\top \in \text{RV}^{12}(2)$ where $X_b^{(n)} \in \text{RV}^6(2)$ and $Y_b^{(n)} \in \text{RV}^6(2)$ represent the features from brain region 1 and brain region 2, respectively, for $b = 1, \dots, B$, $B = 2000$, and $n = 1, \dots, N$, with $N \in \{20, 40\}$. Each matrix $\{Z_b^{(n)}\}_{b=1}^{2000}$ belongs to either cluster-1 or cluster-2. Define $d_n \in \{1, 2\}$ as the cluster label for subject n , then $\{Z_b^{(n)}\}_{b=1}^{2000}$ belonging to cluster- d_n is simulated via the inverse TPDM (i.e., precision matrix), $\Gamma_{d_n}^{-1} := \delta_{d_n} \delta_{d_n}^\top$. Hence, $\delta_{d_n} \in \mathbb{R}^{12 \times 12}$ is the matrix square root of the precision matrix assumed to be the same for all subjects in cluster- d_n .

We simulate the random vector $Z_b^{(n)} \in \text{RV}^{12}(2)$ using the transformed linear operations [Cooley and Thibaud \(2019\)](#). Let $\ell(x) = \log(1 + \exp(x))$, $x \in \mathbb{R}$, and define the transformed linear operators as $x \circ y = \ell(x\ell^{-1}(y))$ and $y \oplus z = \ell(\ell^{-1}(y) + \ell^{-1}(z))$, $y, z \in \mathbb{R}_+$. Moreover, define $V_b^{(n)} \in \mathbb{R}_+^{12}$ to be independent and identically distributed (IID) Frechet(2) random variables. We simulate $\lfloor fN \rfloor$ fuzzy subjects, where $f \in [0, 1]$. For “fuzzy” subject n , define $F_b^{(n)} \stackrel{\text{IID}}{\sim} \text{Bernoulli}(0.5)$ and for “non-fuzzy” subject n , let $F_b^{(n)} = d_n - 1$ for all $b = 1, \dots, 2000$. Then, the simulation model for subject n and channel

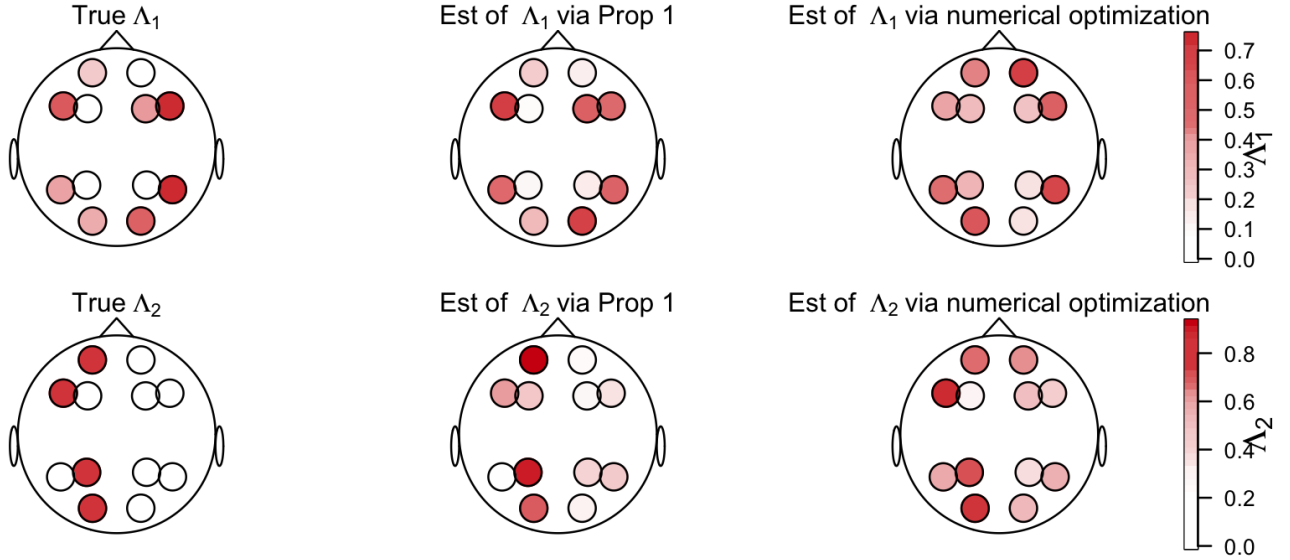


Figure 5: Comparison of Λ_1 estimates from a single simulated $\{Z_b^{(n)}\}_{b=1}^{2000}$ obtained using Proposition 1 (middle panel) and direct numerical optimization (right panel) with the true value of Λ_1 (left panel).

Table 1: Comparison of computational cost of tail-topology estimation using Proposition 1 and standard numerical optimization.

Computational Cost	Estimation via Prop. 1	Estimation via numerical optimization
For Λ_1	0.45 sec	40.83 sec
For Λ_2	0.40 sec	41.52 sec

$j = 1, \dots, D$, at index b is as follows:

$$Z_{j,b}^{(n)} = \delta_{j1}^{(n,b)} \circ V_{1,b}^{(n)} \oplus \delta_{j2}^{(n,b)} \circ V_{2,b}^{(n)} \oplus \dots \oplus \delta_{jD}^{(n,b)} \circ V_{D,b}^{(n)}, \quad (10)$$

where $\delta_{jk}^{(n,b)}$ is the (j,k) -th entry of the matrix $\delta^{(n,b)} = \delta_1(1 - F_b^{(n)}) + \delta_2(F_b^{(n)})$.

We then transform each $\{Z_b^{(n)}\}_{b=1}^{2000}$ to have unit symmetric Pareto margins with shape parameter 2, which satisfies the $RV^1(2)$ property (for details on the symmetric Pareto, see [Jiang et al., 2025a](#)). The analytical solution for the tail-topology of cluster d_n , i.e., $\Lambda_{d_n} \in \mathbb{R}_+^{12}$, is obtained using Proposition 3.1. The true tail-topology, $\Lambda_{d_n}, d_n = 1, 2$, is provided in Figure 5. The accuracy of the clustering methods, given in Equation (9), is obtained for varying $N \in \{20, 40\}$, varying fuzzy parameter $m \in \{1.1, 1.2, 1.5, 1.8, 2.0, 2.2, 2.5\}$, and varying fuzzy proportion $f \in \{0, 0.1\}$.

4.2 Simulation Results

To empirically assess the estimated accuracy, we estimate Λ using two approaches: (1) the approach provided by Proposition 3.1; and (2) using standard numerical optimization based on Equation (3).

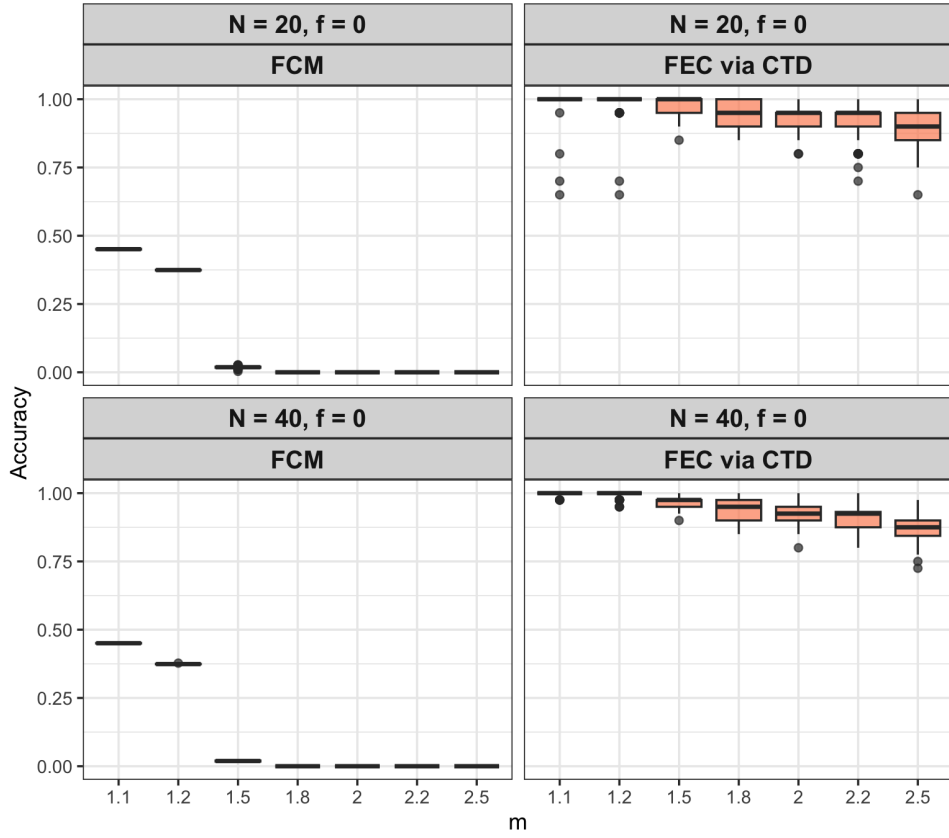


Figure 6: Accuracy of fuzzy extremal clustering (FEC) via the CTD (right) vs fuzzy C-means (FCM, left) clustering at varying levels of fuzzy parameter m , for $N = 20$ (top) and 40 (bottom) subjects with a proportion of fuzzy subjects equal to $f = 0$.

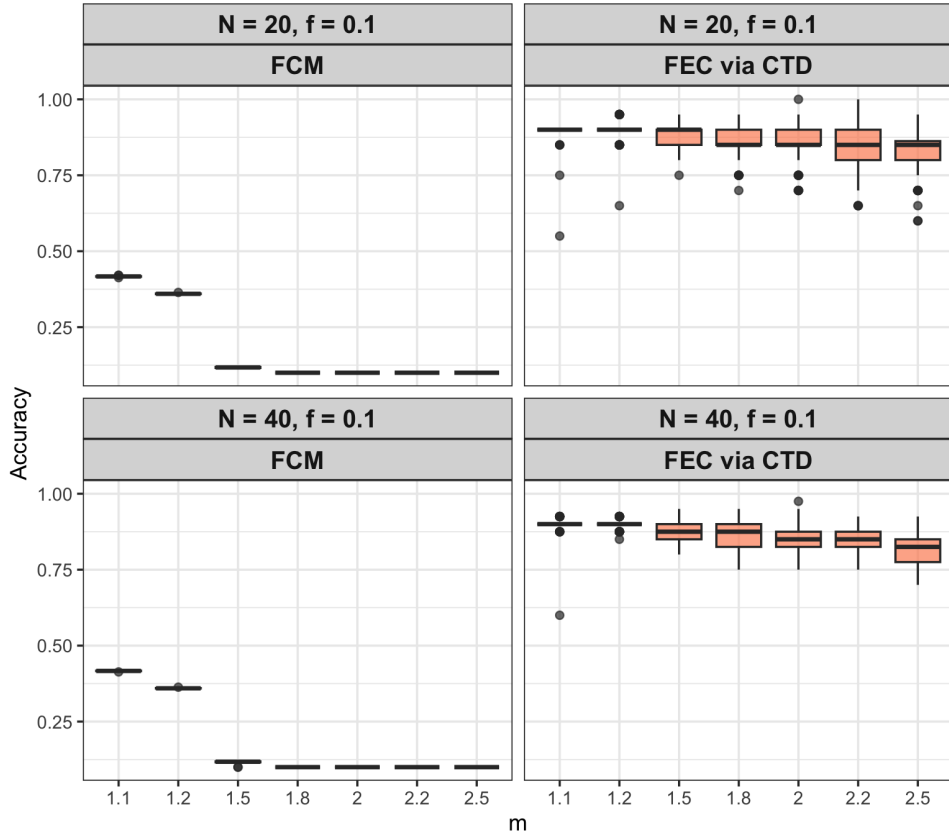


Figure 7: Accuracy of fuzzy extremal clustering (FEC) via the CTD (right) vs fuzzy C-means (FCM, left) clustering at varying levels of fuzzy parameter m , for $N = 20$ (top) and 40 (bottom) subjects with a proportion of fuzzy subjects equal to $f = 0.1$.

Figure 5 compares the two approaches for estimating Λ_1 and Λ_2 . From Figure 5, numerical optimization is not as accurate as the (tail-topology) estimation via the TPDM (as in Proposition 3.1) when compared to the true Λ , which is due to the fact that numerical optimization strongly depends on the choice of initial values in this high-dimensional optimization problem. Moreover, the estimation using Proposition 3.1 has a much lower computational cost (see Table 1). This is because the solution provided by Proposition 3.1 only requires estimation of the TPDM and its eigenvalue decomposition, while numerical optimization has to exhaust all possible combinations and maximizes Equation (3) in order to be accurate. This confirms that the approach based on Proposition 3.1 is both accurate and efficient.

In terms of clustering accuracy, we compared our fuzzy extremal clustering with that of a traditional FCM using the function `cmeans` in the `e1071` R-package (based on work by Bezdek et al., 1984). For each scenario defined in Section 4.1, we run the simulation study 100 times and obtain the accuracy. Figures 6 and 7 summarize the 100 results for each of the scenario. From these figures, fuzzy extremal clustering gives much higher accuracy over traditional FCM for clustering of multivariate regularly varying vectors. Moreover, increasing N leads to slightly more accurate clustering. For $N = 20$ and $f = 0$, the accuracy of fuzzy extremal clustering via CTD ranges approximately from 60% to 100% for m close to 1. When N is increased to 40, the accuracy is at least 90% for the same value of m . Furthermore, when $f = 0$, the highest accuracy is achieved at low values of m , corresponding to clustering behavior that is close to hard clustering. In contrast, when $f > 0$, the maximum accuracy is reached when $m = 2$. This demonstrates the algorithm's ability to effectively cluster data with varying levels of fuzziness.

5 Extremal clustering of neonatal EEG data

We apply our CTD-based extremal clustering method to neonatal EEG periodograms (Section 2.1) denoted as $\{Z_b^{(n)}(\Omega)\}_{b=1}^B \in \mathbb{R}_+^{D \times B}$, for each subject $n = 1, \dots, 14$ and for each fundamental frequency band, Ω , i.e., delta, theta, alpha, beta and gamma. Figure 8 plots the EEG periodograms of a subject for five frequency bands. From this figure, gamma-band periodograms appear to have a relatively more heavy-tailed behavior. For each subject n and a fixed Ω , we standardize the data to have common margins.

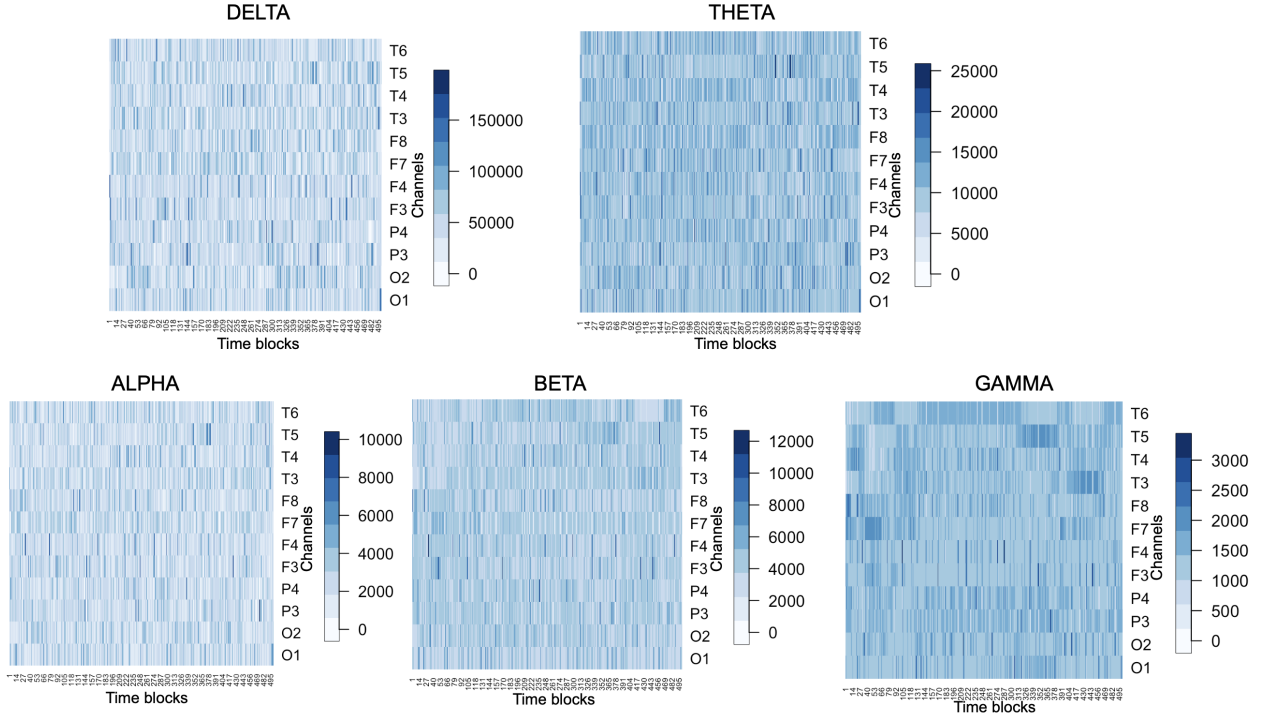


Figure 8: First 500 block-varying periodograms, $\{Z_b^{(n)}(\Omega)\}_{b=1}^{500}$, for a single subject n and for all five frequency bands, Ω , namely, delta, theta, alpha, beta, and gamma.

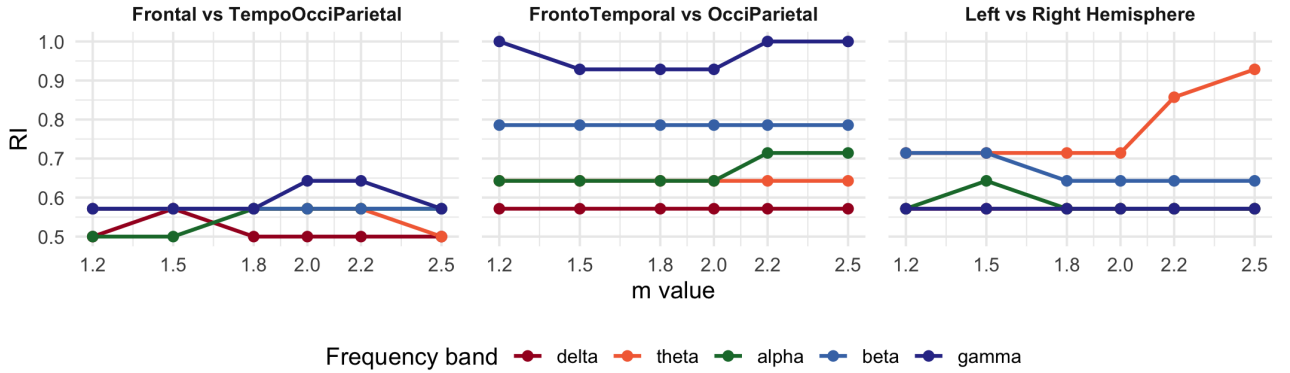


Figure 9: Accuracy of our fuzzy extremal clustering (CTD-based) evaluated for different fuzzy parameter values m (x-axis), different frequency bands, Ω (colors), and different connectivity regions (panels).

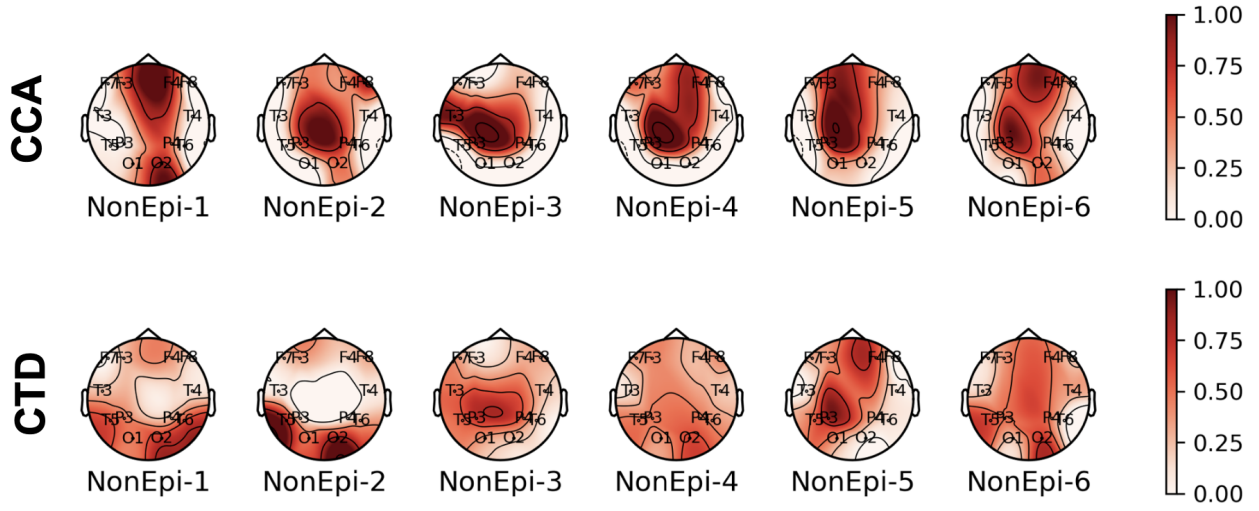


Figure 10: Tomomaps (using mne Python package, see [Gürsoy et al., 2014](#)) of CCA estimates, $|\hat{\Lambda}_0^{(n)}|$ (first row) and tail-topology, $\hat{\Lambda}_n$ (second row), of six non-epileptic neonates at the gamma band for FrontoTemporal-vs-OcciParietal connectivity. Darker color represents higher magnitude for channels $j = 1, \dots, 12$, labeled F3, F7, F4, F8, T3, T4, T5, T6, P3, P4, O1, O2.

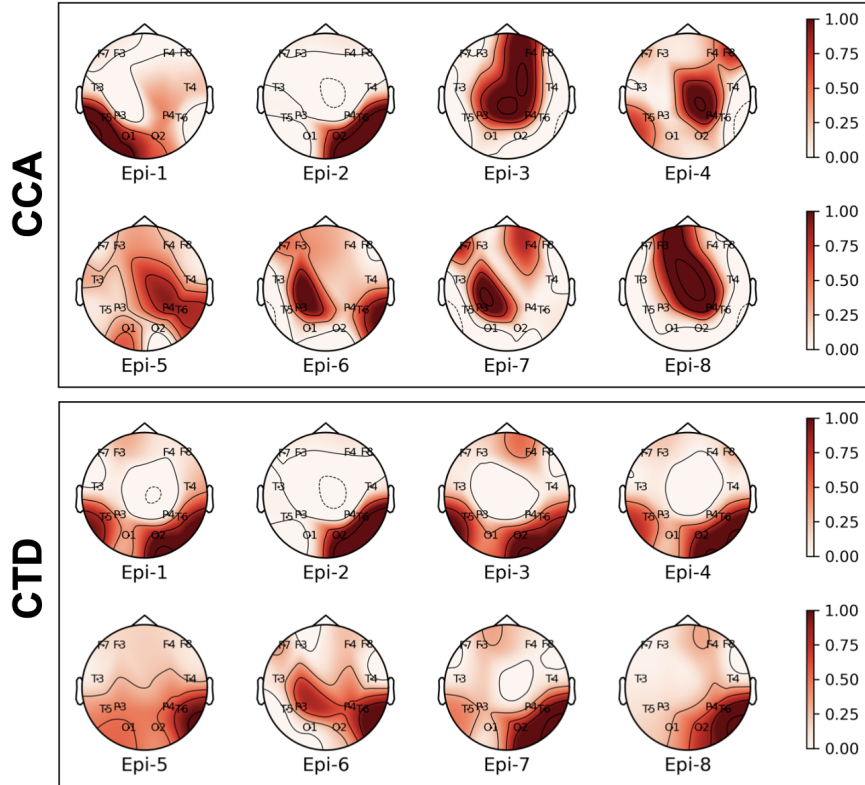


Figure 11: Tomomaps (using mne Python package, see [Gürsoy et al., 2014](#)) of CCA estimates, $|\hat{\Lambda}_0^{(n)}|$ (first and second row), and tail-topology, $\hat{\Lambda}_n$ (third and fourth row), of eight epileptic neonates with primary localization on *right hemisphere* at the gamma band for FrontoTemporal-vs-OcciParietal connectivity. Darker color represents higher magnitude for channels $j = 1, \dots, 12$, labeled F3, F7, F4, F8, T3, T4, T5, T6, P3, P4, O1, O2.

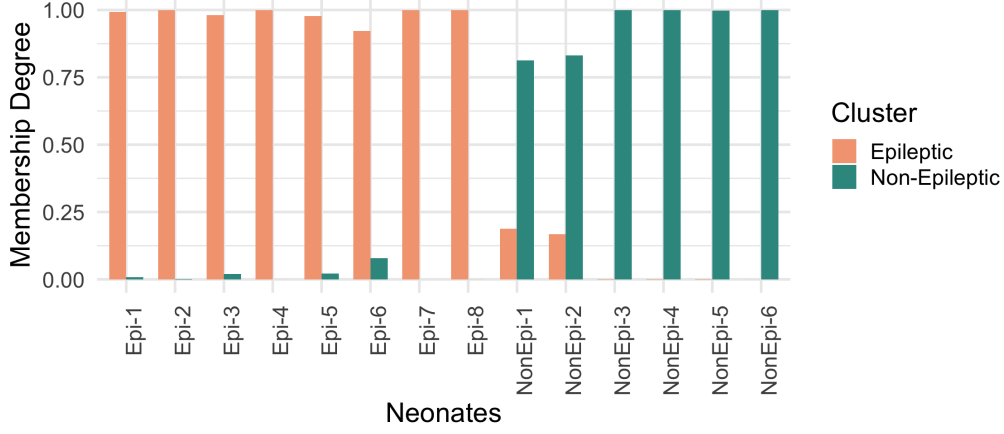


Figure 12: Membership matrix, U , of our fuzzy extremal clustering for $m = 1.2$ at the gamma-band. The orange bars represent the degree of epileptic-membership $\{U_{n,1}\}_{n=1}^{14}$, while green bars represent the degree of non-epileptic-membership of a subject, $\{U_{n,2}\}_{n=1}^{14}$.

As EEG frequency bands are linked to human cognitive development (Srinivasan, 2007), we aim to identify the frequency band that best distinguishes epileptic and non-epileptic neonates. Figure 9 shows the accuracy (see Equation (9)) of our clustering results based on experts annotations/labels, for each frequency band and different fuzzy-parameters $m \in \{1.2, 1.5, 1.8, 2.0, 2.5\}$. Comparing Figures 4 and 9 for FrontoTemporal-vs-OcciParietal and Left-vs-Right Hemisphere, our method achieves higher clustering accuracy (see Figure 9) than standard CCA. For FrontoTemporal-vs-OcciParietal connectivity and $m = 1.2$, our method identifies the gamma band as the best band for discriminating between epileptic and non-epileptic neonates (with an accuracy of 100%). This result is in-line with the findings of Guerrero et al. (2023) who highlighted the gamma band as the most relevant frequency for exploring tail-dependence of (seizure) EEG data. At $m = 2.5$, the CTD-based clustering of connectivity of Left-vs-Right Hemisphere at the theta-band provides more than 90% accuracy, which implies that there are EEGs for fuzzy-neonates or neonates that exhibit tail-dependence properties of both clusters. The theta band is one of the components of burst-suppression patterns that are also found in normal EEG recordings (Dulac, 2013; Talento et al., 2025). This is one of many *potential* factors that could bring out fuzziness between the clusters under Left-vs-Right Hemisphere connectivity. The Frontal-vs-TempoOcciParietal connectivity still has the lowest accuracy in discriminating epileptic and non-epileptic neonates.

Highlights: novel results on extremal dependence of amplitudes. In Figures 10 (second row) and 11 (third and fourth row), we visualize the FrontoTemporal-vs-OcciParietal tail-topology at the gamma band (with $m = 1.2$) using tomomaps in mne Python package (tomomaps in Python use

Gaussian kernel-based spatial smoothing; for details of tomomaps, see [Gürsoy et al., 2014](#)). The tail-topology displayed in Figures 10 (second row) and 11 (third and fourth row) represents the absolute values of eigenvectors $\{\Lambda_n\}_{n=1}^{14}$, with the FrontoTemporal channels populating $\{X_b\}_{b=1}^{2000}$ and the OcciParietal channels populating $\{Y_b\}_{b=1}^{2000}$. Figure 11 (third and fourth row) shows clear and unique FrontoTemporal-vs-OcciParietal tail-topology of epileptic patients in contrast with that of non-epileptic patients (see Figure 10, second row). The proposed method captures features about the extremes that have not been previously reported. In particular, the method demonstrates that the maximal tail-dependence between FrontoTemporal-vs-OcciParietal of epileptic patients is mostly driven by right Temporal and OcciParietal channels (i.e., P4, O6, and T6). Note that these neonates had primary localization at the right-hemisphere, and this feature is revealed only in the tails of gamma band amplitudes. Moreover, results from our proposed method confirm that the tail connectivity of neonatal EEG data from [Stevenson et al. \(2019\)](#) is distinct and more homogeneous (within clusters) compared to the bulk connectivity depicted in Figures 10 and 11. Figure 12 shows the estimated membership degree, $U \in [0, 1]^{14 \times 2}$, of each neonate for the two clusters. As $m = 1.2$, we observe that the proposed method produces a clear separation between the clusters, with only two non-epileptic neonates (NonEpi-1 and NonEpi-2) exhibiting over 10% similarity with the epileptic cluster. The remaining subjects show near-perfect membership to the correct cluster. Referring back to Figure 10 (second row), both NonEpi-1 and NonEpi-2 are characterized by relatively substantial contributions from the Temporal and OcciParietal channels (i.e., P4, O6, and T6); however, their overall similarity to the other non-epileptic neonates remains stronger.

6 Conclusion

In this paper, we have developed a novel method that addresses the problem of clustering extreme events—which is prevalent in many areas including climate and finance, as well as biology and neuroscience. However, this task is non-trivial, especially when data are jointly heavy-tailed. In this paper, we extract unique features lurking at the tails of the distribution which enhance discrimination of extreme events, and paves the way for representation learning of rare events. In particular, we develop a novel way of characterizing multivariate tail-connectivity based on multivariate regular-variation ([Resnick, 2007](#)). Our proposed canonical tail dependence (CTD) measure is the first of its kind to offer tail-topology of connectivity between two random vectors. The CTD finds the combination of variables

that provide the maximal tail-dependence between groups—we solve for unique weights attributed to each component that achieves the maximal tail-dependence of two linear combinations. These weights form the tail-topology that facilitates visualization and interpretation of clusters, highlighting a major advantage of our method.

We provide an efficient way of estimating the CTD through the tail pairwise dependence matrix (Cooley and Thibaud, 2019). We embed the CTD estimates into the fuzzy C-means algorithm, thereby developing a novel *soft clustering of multivariate extremes*. The application to neonatal EEGs revealed interesting tail-topology of epileptic and non-epileptic neonates. At the gamma band, channels in non-epileptic patients contribute equally to the maximal tail-dependence (or CTD), while few specific channels in epileptic patients are likely to be the key drivers of the CTD.

Our method is currently limited to stationary but jointly heavy-tailed signals. Moreover, the CTD considers linear combinations of regularly varying variables. Our future work will focus on weakening the stationarity assumption by using wavelets (Graps, 1995; Rhif et al., 2019) as a basis, instead of Fourier coefficients. Additionally, one may also extend our approach to the case of asymptotic independence of signals, i.e., hidden regular variation (Resnick, 2002). Another interesting direction is to develop a data-driven approach to select the optimal groups that maximize clustering accuracy, such as fuzzy co-clustering (Kummamuru et al., 2003). Furthermore, future studies may consider the maximal extremal dependence between non-linear combinations of vectors. This could utilize deep learning which has already seen effective use in capturing complex tail-dependencies (see e.g., De Monte et al., 2025; Shao et al., 2025; Hu and Castro-Camilo, 2025), and has already seen use in canonical correlation analyses (Andrew et al., 2013).

Acknowledgments

The authors would like to thank Dan Cooley for helpful discussions and access to a working article.

References

- Andrew, G., Arora, R., Bilmes, J., and Livescu, K. (2013). Deep canonical correlation analysis. In International Conference on Machine Learning, pages 1247–1255. PMLR.
- Bezdek, J. C., Ehrlich, R., and Full, W. (1984). FCM: The fuzzy c-means clustering algorithm. Computers & Geosciences, 10(2-3):191–203.
- Bigdely-Shamlo, N., Mullen, T., Kothe, C., Su, K.-M., and Robbins, K. A. (2015). The PREP pipeline: standardized preprocessing for large-scale EEG analysis. Frontiers in Neuroinformatics, 9:16.
- Brillinger, D. R. (1969). The canonical analysis of stationary time series. Multivariate Analysis, 2:331–350.
- Cooley, D. (2025+). Properties of the tail pairwise dependence matrix. Working draft.
- Cooley, D. and Thibaud, E. (2019). Decompositions of dependence for high-dimensional extremes. Biometrika, 106(3):587–604.
- De Monte, L., Huser, R., Papastathopoulos, I., and Richards, J. (2025). Generative modelling of multivariate geometric extremes using normalising flows. arXiv preprint arXiv:2505.02957.
- Donofry, S. D., Stillman, C. M., and Erickson, K. I. (2020). A review of the relationship between eating behavior, obesity and functional brain network organization. Social Cognitive and Affective Neuroscience, 15(10):1157–1181.
- Dulac, O. (2013). Epileptic encephalopathy with suppression-bursts and nonketotic hyperglycinemia. Handbook of Clinical Neurology, 113:1785–1797.
- D’Urso, P. and Maharaj, E. A. (2012). Wavelets-based clustering of multivariate time series. Fuzzy Sets and Systems, 193:33–61.
- D’Urso, P., Maharaj, E. A., and Alonso, A. M. (2017). Fuzzy clustering of time series using extremes. Fuzzy Sets and Systems, 318:56–79.
- Elsom, H. and Pawley, M. (2025). Extreme value statistics for analysing simulated environmental extremes. Extremes, 28(1):47–73.

- Gong, Y., Zhong, P., Opitz, T., and Huser, R. (2024). Partial tail-correlation coefficient applied to extremal-network learning. Technometrics, 66(3):331–346.
- Goutte, C., Hansen, L. K., Liptrot, M. G., and Rostrup, E. (2001). Feature-space clustering for fMRI meta-analysis. Human Brain Mapping, 13(3):165–183.
- Graps, A. (1995). An introduction to wavelets. IEEE Computational Science and Engineering, 2(2):50–61.
- Guerrero, M. B., Huser, R., and Ombao, H. (2023). Conex–Connect: Learning patterns in extremal brain connectivity from multichannel EEG data. The Annals of Applied Statistics, 17(1):178–198.
- Guerrero, M. B., Ombao, H., and Huser, R. (2022). Club Exco: clustering brain extreme communities from multi-channel EEG data. arXiv:2212.04338.
- Gürsoy, D., De Carlo, F., Xiao, X., and Jacobsen, C. (2014). TomoPy: a framework for the analysis of synchrotron tomographic data. Journal of Synchrotron Radiation, 21(5):1188–1193.
- Han, C. E., Yoo, S. W., Seo, S. W., Na, D. L., and Seong, J.-K. (2013). Cluster-based statistics for brain connectivity in correlation with behavioral measures. PLoS One, 8(8):e72332.
- He, H. and Tan, Y. (2018). Unsupervised classification of multivariate time series using VPCA and fuzzy clustering with spatial weighted matrix distance. IEEE Transactions on Cybernetics, 50(3):1096–1105.
- Hotelling, H. (1936). Relations between two sets of variates. Biometrika, 28(3):321–377.
- Hu, C. and Castro-Camilo, D. (2025). GPDFlow: Generative multivariate threshold exceedance modeling via normalizing flows. arXiv preprint arXiv:2503.11822.
- Huang, H., Meng, F., Zhou, S., Jiang, F., and Manogaran, G. (2019). Brain image segmentation based on FCM clustering algorithm and rough set. IEEE Access, 7:12386–12396.
- Janßen, A. and Wan, P. (2020). K-means clustering of extremes. Electronic Journal of Statistics, 14(1):1211–1233.
- Jiang, J., Richards, J., Huser, R., and Bolin, D. (2025a). The efficient tail hypothesis: An extreme value perspective on market efficiency. Journal of Business & Economic Statistics, (To appear).

- Jiang, J., Richards, J., Huser, R., and Bolin, D. (2025b). Separation-based causal discovery for extremes. arXiv preprint arXiv:2505.08008.
- Jiang, Y., Cooley, D., and Wehner, M. F. (2020). Principal component analysis for extremes and application to US precipitation. Journal of Climate, 33(15):6441–6451.
- Kummamuru, K., Dhawale, A., and Krishnapuram, R. (2003). Fuzzy co-clustering of documents and keywords. In The 12th IEEE International Conference on Fuzzy Systems, 2003. FUZZ'03., volume 2, pages 772–777. IEEE.
- Larsson, M. and Resnick, S. I. (2012). Extremal dependence measure and extremogram: the regularly varying case. Extremes, 15(2):231–256.
- Liu, X., Zhu, X.-H., Qiu, P., and Chen, W. (2012). A correlation-matrix-based hierarchical clustering method for functional connectivity analysis. Journal of Neuroscience Methods, 211(1):94–102.
- López-Oriona, Á., Vilar, J. A., and D’Urso, P. (2022). Quantile-based fuzzy clustering of multivariate time series in the frequency domain. Fuzzy Sets and Systems, 443:115–154.
- Lucińska, M. (2014). A spectral clustering algorithm based on eigenvector localization. In International Conference on Artificial Intelligence and Soft Computing, pages 749–759. Springer.
- Ma, Z., Talento, M. S., Sun, Y., and Ombao, H. (2025a). Fuzzcoh: Robust canonical coherence-based fuzzy clustering of multivariate time series. arXiv preprint arXiv:2506.22861.
- Ma, Z., Ángel López-Oriona, Ombao, H., and Sun, Y. (2025b). FCPCA: Fuzzy clustering of high-dimensional time series based on common principal component analysis. International Journal of Approximate Reasoning, 187:109552.
- Mardia, K. and Kent, J. (1979). Multivariate analysis. New York: Academic Press.
- McGonigle, E. T., Pawley, M., Richards, J., and Rohrbeck, C. (2025). MOPED: A moving sum method for change point detection in pairwise extremal dependence. arXiv preprint arXiv:2509.00585.
- Meyer, N. and Wintenberger, O. (2024). Multivariate sparse clustering for extremes. Journal of the American Statistical Association, 119(547):1911–1922.

- Mizrahi, E. M. and Clancy, R. R. (2000). Neonatal seizures: Early-onset seizure syndromes and their consequences for development. Mental Retardation and Developmental Disabilities Research Reviews, 6(4):229–241.
- Murugappan, M., Rizon, M., Nagarajan, R., Yaacob, S., Zunaidi, I., and Hazry, D. (2007). EEG feature extraction for classifying emotions using FCM and FKM. International Journal of Computers and Communications, 1(2):21–25.
- NIH (2023). Epilepsy and seizures. <https://www.ninds.nih.gov/health-information/disorders/epilepsy-and-seizures>. Accessed: 2025-09-28.
- Ombao, H. and Pinto, M. (2024). Spectral dependence. Econometrics and Statistics, 32:122–159.
- O’Toole, P., Rohrbeck, C., and Richards, J. (2025). Clustering of multivariate tail dependence using conditional methods. arXiv preprint arXiv:2510.20424.
- Panayiotopoulos, C. (2005). Neonatal seizures and neonatal syndromes. In The Epilepsies: Seizures, Syndromes and Management. Bladon Medical Publishing.
- Pinto-Orellana, M. and Lopour, B. (2024). Connectivity of high-frequency bursts as soz localization biomarker. Frontiers in Network Physiology, 4:1441998.
- Pisani, F., Spagnoli, C., Falsaperla, R., Nagarajan, L., and Ramantani, G. (2021). Seizures in the neonate: A review of etiologies and outcomes. Seizure, 85:48–56.
- Rawashdeh, M. and Ralescu, A. (2012). Crisp and fuzzy cluster validity: Generalized intra-inter silhouette index. In 2012 Annual Meeting of the North American Fuzzy Information Processing Society (NAFIPS), pages 1–6. IEEE.
- Redondo, P. V., Guerrero, M. B., Huser, R., and Ombao, H. (2025). Statistics of extremes for neuroscience. In de Carvalho, M., Huser, R., Naveau, P., and Reich, B., editors, In the Handbook of Statistics of Extremes, number To appear. Chapman & Hall/CRC Press, Boca Raton, FL.
- Resnick, S. (2002). Hidden regular variation, second order regular variation and asymptotic independence. Extremes, 5(4):303–336.
- Resnick, S. (2004). The extremal dependence measure and asymptotic independence. Stochastic Models, 20(2):205–227.

- Resnick, S. I. (2007). Heavy-tail Phenomena: Probabilistic and Statistical Modeling. Springer Science & Business Media.
- Rhif, M., Ben Abbes, A., Farah, I. R., Martínez, B., and Sang, Y. (2019). Wavelet transform application for/in non-stationary time-series analysis: A review. Applied Sciences, 9(7):1345.
- Richards, J., Alotaibi, N., Cisneros, D., Gong, Y., Guerrero, M. B., Redondo, P., and Shao, X. (2025). Modern extreme value statistics for utopian extremes. Extremes, 28(1):149–171.
- Russell, B. T., Cooley, D. S., Porter, W. C., Reich, B. J., and Heald, C. L. (2016). Data mining to investigate the meteorological drivers for extreme ground level ozone events.
- Sandoval Karamian, A. G. and Wusthoff, C. J. (2021). Current and future uses of continuous EEG in the NICU. Frontiers in Pediatrics, 9:768670.
- Seghier, M. L., Friston, K. J., and Price, C. J. (2007). Detecting subject-specific activations using fuzzy clustering. Neuroimage, 36(3):594–605.
- Shao, X., Richards, J., and Huser, R. (2025). Modeling nonstationary extremal dependence via deep spatial deformations. arXiv preprint arXiv:2505.12548.
- Shapson-Coe, A., Januszewski, M., Berger, D. R., Pope, A., Wu, Y., Blakely, T., Schalek, R. L., Li, P. H., Wang, S., Maitin-Shepard, J., et al. (2024). A petavoxel fragment of human cerebral cortex reconstructed at nanoscale resolution. Science, 384(6696):eadk4858.
- Shumway, R. H. and Stoffer, D. S. (2000). Time Series Analysis and its Applications. Forth edition, Springer, New York.
- Srinivasan, N. (2007). Cognitive neuroscience of creativity: EEG based approaches. Methods, 42(1):109–116.
- Stevenson, N. J., Tapani, K., Lauronen, L., and Vanhatalo, S. (2019). A dataset of neonatal EEG recordings with seizure annotations. Scientific Data, 6(1):1–8.
- Talento, M. S. D., Richards, J., Pinto-Orellana, M., Huser, R., and Ombao, H. C. (2025). Spectral extremal connectivity of two-state seizure brain waves. arXiv:2503.04169.

- Talento, M. S. D., Roy, S., Vallejo, T. R., Ibrahim, L. A., and Ombao, H. C. (2024). Kencoh: A ranked-based canonical coherence. arXiv preprint arXiv:2412.10521.
- Tononi, G., McIntosh, A. R., Russell, D. P., and Edelman, G. M. (1998). Functional clustering: identifying strongly interactive brain regions in neuroimaging data. Neuroimage, 7(2):133–149.
- Wang, X.-Y. and Bu, J. (2010). A fast and robust image segmentation using FCM with spatial information. Digital Signal Processing, 20(4):1173–1182.
- Zadeh, L. A., Klir, G. J., and Yuan, B. (1996). Fuzzy Sets, Fuzzy Logic, and Fuzzy Systems: Selected Papers. World scientific, Farrer Rd, Singapore.
- Zhang, X., Ning, Y., Li, X., and Zhang, C. (2021). Anti-noise FCM image segmentation method based on quadratic polynomial. Signal Processing, 178:107767.
- Zheng, B. S., Murugappan, M., and Yaacob, S. (2013). FCM clustering of emotional stress using ECG features. In 2013 International Conference on Communication and Signal Processing, pages 305–309. IEEE.